JOINT EUROPEAN TORUS

JET–P(90)68

M.A. Kovanen, W.G.F. Core, T. Hellsten
and JET Team

Finite Orbit Effects in ICRF Heated Tokamak Plasmas

Finite Orbit Effects in ICRF Heated Tokamak Plasmas

M.A. Kovanen[1], W.G.F. Core, T. Hellsten[2]
and JET Team*

JET-Joint Undertaking, Culham Science Centre, OX14 3DB, Abingdon, UK

[1]Lappeenranta University of Technology, Finland and National Research Council for Technology, The Academy of Finland
[2]Royal Institute of Technology, Stockholm, Sweden.
** See Appendix 1*

Preprint of Paper to be submitted for publication in
Nuclear Fusion

Finite Orbit Effects in ICRF Heated Tokamak Plasmas

M.A. Kovanen* , W.G.F. Core

JET Joint Undertaking, Abingdon, Oxon. OX14 3EA, UK

and T. Hellsten

Royal Institute of Technology, Stockholm, Sweden

ABSTRACT

A Monte-Carlo investigation of ion cyclotron resonance heating of tokamak plasmas is undertaken to study the effect of finite banana width orbits on the efficiency of the heating process. For minority heating schemes with peaked power deposition profiles, there is a significant reduction in absorbed and transferred power in the centre of the discharge compared with zero orbit width calculations. The broader power transfer profiles give rise to a large reduction of tail energy in the centre while the total fast ion energy content and the total thermonuclear yield are less affected. The reduction of the power absorption in the centre for fixed wave field profiles arise because of the broadening of the orbits and the enhanced diffusion and drift of the heated ions. The importance of these effects is assessed.

I. INTRODUCTION

High power radio frequency waves in the ion cyclotron range of frequencies (ICRF) are one of the most promising methods of heating tokamak

---

* Lappeenranta University of Technology, Finland and National Research Council for Technology, The Academy of Finland.

plasmas to thermonuclear temperature. The damping of the fast magnetosonic wave on the minority ion species leads to the development of a non-Maxwellian velocity distribution which is highly anisotropic with a significant fraction of the resonating particles trapped in the toroidal magnetic field. In the large tokamaks currently operating in which the wave fields are strongly focused on or near the magnetic axis, resonant ions with energies in the MeV range have been produced. These ions have large Larmor radii, and those particles which move on banana orbits passing close to the centre of the discharge make large radial excursions across the minor radius of the torus. This modifies the power absorption, and consequently the wave fields. Since the transfer of energy from the ions takes place over the complete orbit and the absorption of wave power occurs only during its passage through the cyclotron resonance layer, the radial excursion of the resonating ions also leads to a broadening of the plasma heating profile. The orbit effects are not limited to high power heating cases only, as even moderate heating power can provide high enough power density if the minority concentration is sufficiently low. In present large tokamaks operating in the high temperature regime the slowing down time is long, typically ~ 1 sec., thus favouring the creation of high energy particles by ICRH. On the other hand, in small tokamaks with low plasma currents, even reasonably low ion energy can result in significant resonant particle loss from the plasma. The effects of the finite orbit width are important not only to the theoretical understanding of the heating process but also in the interpretation of experimental data, and merits a detailed study.

Hitherto most ion cyclotron resonance heating studies of tokamak plasmas have been done in the zero banana width approximation limit. The evolution of the resonant ion distribution function in velocity space due to the combined effects of Coulomb scattering on the background ions and electrons and the interaction with the RF wave fields can then be obtained by solving a quasilinear Fokker-Planck equation. Using this solution procedure the heating

process has been treated extensively both analytically [1-6] and numerically [7,8] in the literature. These methods become unsatisfactory for the study of heating systems in which orbit effects are important. To formulate a realistic Fokker-Planck procedure for the problem which includes finite orbit effects, the spatial properties of the plasma, and geometry of the vessel becomes difficult. An attempt to include finite orbit effects on the ICRF heating process has recently been undertaken [9]. These authors used the Stix model for the energetic particle distribution function and a simplified system of equations to describe the particle trajectories within the plasma. This approach is clearly inadequate as it is only valid in the zero banana width approximation, cannot assess loss-cone effects and does not include the effect of the E_- wave electric field component on the development of the high energy tail. Furthermore, the important effects of neoclassical and RF-driven transport processes on the distribution of energetic particles within the discharge cannot be included in this method of treatment. In order to rectify this situation an alternative solution procedure, such as that afforded by the Monte-Carlo method, is required. This method has great flexibility and can be used to do detailed studies of the heating process which cannot be readily done using alternative methods.

In this work, the finite-orbit width effects have been studied using the orbit following Monte-Carlo code HECTOR [10] which includes the usual Coulomb collisional processes and wave-particle interaction by ion cyclotron heating. The results are compared with a semi-analytical model [6] in which the power deposition and velocity distribution are calculated self-consistently in the zero orbit width limit. The structure of this paper is as follows. In Section 2 we discuss and classify the orbit topology of the ICRF heated minority ions. The numerical model is described in Section 3. The results of the numerical analysis, showing significant deviation in minority ion density, power absorption and transfer to the background plasma and mean energy profiles, among others,

compared with the zero orbit width limit calculations, are presented and discussed in Section 4. Finally, Section 5 contains the conclusions.

2. PRELIMINARY PHYSICS CONSIDERATIONS

As an ion passes through the cyclotron layer and undergoes resonant interaction with the wave fields an incremental change in velocity takes place. The sign and magnitude of the velocity increment depends on the phase between the gyro motion of the ion and the wave fields. If the wave propagation vector has a component parallel to the magnetic field, then the resonating ion will acquire a change in the velocity parallel as well as perpendicular to the magnetic field. However, the former change is much smaller than the latter, thus resulting in a strongly anisotropic velocity distribution with a large population of highly energetic trapped ions. When the ions in the passing region of velocity space are scattered by the RF wave fields into the trapped particle region a neoclassical type diffusion occurs.

If we neglect the change in parallel velocity due to pitch angle scattering and cyclotron absorption, it follows from the conservation of the toroidal angular momentum P_ϕ, the magnetic moment μ and the particle energy E, that as the perpendicular velocity increases the turning points of the trapped ions are driven closer to the cyclotron resonance. From these invariants we can derive the intersection points of the drift orbit with the cyclotron resonance layer. Thus, we have

$$\psi_i = \psi_t + \frac{mR_iB_\phi}{qB} v_{\|}, \tag{1}$$

where ψ is the poloidal flux function, m and q are the particle mass and charge, respectively, R is the major radius, B_ϕ and B are the toroidal and total magnetic field strengths, respectively and $v_{\|} = \pm\left[\frac{2}{m}(E-\mu B)\right]^{1/2}$ is the parallel component of the particle velocity. Subscripts i and t refer to the intersection points and the turning point ($v_{\|} = 0$), respectively. This equation shows that the intersection

points of the inner and the outer branch of the drift orbit are within the same distance from the turning point in flux coordinates. However, as the flux function is related to the radial coordinate by $\psi \sim r^2$, the radial displacement of the inner and outer intersection point from the turning point is not the same. Thus, when the particle energy increases the inner branch takes longer steps towards the small radius r_i than the outer branch takes outwards. When the wave field has a peaked profile the effect is substantially increased. Although particles initially in the central region contribute to the density mainly further out, more particle orbits further out will expand and increase the central density. Furthermore, as the turning points of the trapped particles are driven close to the resonance layer, the fraction of time spent in this layer compared to the time of completing the whole orbit is increased and more power is absorbed. Thus, a substantial increase in power absorption and minority density near the centre region will occur, unless the banana drift and the diffusion due to finite orbit effects limit it. The banana drift arises from particles being in different parts of the velocity space on the inner and outer branch of the orbit. The parallel velocity $v_{\|}$ undergoes a sign change as it moves from the inner to the outer branch, and the average value of $|v_{\|}|$ is smaller on the inner branch. Thus, for a given change in the particle velocity Δv, the change $|\Delta v_{\|}|$ and consequently $|\Delta P_\phi|$ are smaller on the inner than on the outer branch of the orbit. As the increase in P_ϕ on the inner branch of the orbit is not large enough to compensate for the decrease of P_ϕ on the outer branch, a radial drift of the banana orbit occurs. Banana drift exists even when temperature and density profiles are flat. The profile gradients further enhance this process due to the different slowing down rates on the inner and outer branches, and as the distance between the turning points of the orbit is shorter along the inner branch the total change in P_ϕ is substantially larger on the outer branch.

Let us now consider the processes which could lead to further depletion of the minority density near axis. If the toroidal wave number is different from

zero the resonating ions also receive a change in their parallel velocity component as they pass through the cyclotron resonance layer. The change in the toroidal angular momentum is

$$\Delta P_\phi = mR_i B_\phi \Delta v_\parallel / B. \tag{2}$$

The displacement of the turning points for trapped ions can then be obtained from

$$\Delta \psi_t = \frac{\Delta P_\phi}{q}, \tag{3}$$

and the corresponding change in the other intersection points with the cyclotron resonance from

$$\Delta \psi_i = \Delta \psi_t + \frac{mR_i B_\phi}{qB} \Delta v_\parallel. \tag{4}$$

The random displacement of the turning point and the intersection points with the cyclotron resonance leads to spatial diffusion. In cases of an asymmetric wave spectrum there is also spatial drift.

The diffusion problem was recently studied in the small banana width approximation by solving a diffusion equation in real and velocity space. Results indicate a pump out of ions from the central regions of high power density and the formation of hollow resonant ion density profiles [11,12]. In these investigations, as well as in the present study, it is assumed that the different changes in velocity at the cyclotron resonance are uncorrelated. This will be the case if the gyro phase of the ions are decorrelated through Coulomb scattering on the plasma ions and electrons during consecutive passes through the cyclotron layer. For high temperature plasmas of low density this is not always fulfilled and there results a superadiabatic behaviour of the ions characterised by a transfer of power between the ions and wave field without power absorption. However, if the wave field is sufficiently high the superadiabaticity is destroyed and stochastic heating occurs [13].

3. NUMERICAL PROCEDURE

HECTOR is an orbit following code for the study of charged particles in axisymmetric tokamak plasmas in which the particle trajectories are traced in the invariant (P_ϕ, μ, v) space. Collisions are taken into account by calculating new values of the particle velocity, the magnetic momentum, and the toroidal canonical angular momentum after each time step.

$$\begin{aligned} v &\rightarrow v + \Delta v \\ \mu &\rightarrow \mu + \Delta\mu \\ P_\phi &\rightarrow P_\phi + \Delta P_\phi, \end{aligned} \tag{5}$$

where

$$\begin{aligned} \Delta\mu &= \frac{m}{2B}\left(2v\Delta v + (\Delta v)^2 - 2v_{\|}\Delta v_{\|} - (\Delta v_{\|})^2\right) \\ \Delta P_\phi &= mRB_\phi \Delta v_{\|}/B \end{aligned} \tag{6}$$

are the incremental changes in magnetic moment ($\Delta\mu$) and toroidal canonical momentum (ΔP_ϕ) due to the cumulative effects of dynamical friction, pitch angle scattering, energy diffusion, and RF-wave interaction, and Δv and $\Delta v_{\|}$ are the incremental changes in particle velocity and it's parallel component, occurring during the time step. In order to achieve energy conservation it is necessary that the second order differentials appearing in Eq. (6) are included in the numerical procedure.

Following the analytical treatment of the Fokker-Planck equation by Stix [1], one can write the change in particle velocity due to friction occurring during a time interval Δt,

$$\Delta v = -\sum_f \left(C_f \frac{m}{2kT_f} G(\ell_f v) \Delta t \right), \tag{9}$$

where

$$C_f = 8\pi n_f Z_f^2 Z^2 e^4 \ell n / m^2$$
$$\ell_f^2 = m_f / (2kT_f)$$
$$G(x) = \frac{\phi(x) - x\phi'(x)}{2x^2} \tag{10}$$
$$\phi(x) = \frac{2}{\pi^{1/2}} \int_0^x e^{-y^2} dy$$

and the subscript f designates the background field particles, ions and electrons. The change in the parallel velocity due to this change in velocity is then given by

$$\Delta v_{\|} = \xi \Delta v, \tag{11}$$

where ξ is the pitch, the cosine of the pitch angle.

Boozer and Kuo-Petravic [14] give a simple Monte-Carlo equivalent Lorenz collision operator. The change in the parallel velocity due to pitch angle scattering during Δt is $\Delta v_{\|} = v\Delta\xi$, where

$$\Delta\xi = v\Delta t\xi + \delta_1 \left[(1 - \xi^2) v \Delta t \right]^{1/2}, \tag{12}$$

$\delta_1 = \pm 1$ with equal probabilities, and the collision frequency ν given by Spitzer [15] is

$$\nu = \frac{1}{2v^3} \sum_f C_f \left[\phi(\ell_f v) - G(\ell_f v) \right]. \tag{13}$$

These authors also give an energy scattering equivalent of the Lorentz scattering operator. The change in particle energy during Δt is

$$\Delta E = -2\nu_E \Delta t \left[E - \left(\frac{3}{2} + \frac{E}{\nu_E} \frac{d\nu_E}{dE} \right) T \right] + \delta_2 \left[4TE(\nu_E \Delta t) \right]^{1/2} \tag{14}$$

where $\delta_2 = \pm 1$ with equal probabilities, and T is the background Maxwellian temperature. The energy scattering frequency is [15]

$$\nu_E = \frac{1}{v^3} \sum_f \left[C_f G(\ell_f v) (\ell_f v)^2 \right]. \tag{15}$$

The change in particle velocity then becomes

$$\Delta v = \left[v^2 + \frac{2}{m} \Delta E \right]^{1/2} - v, \tag{16}$$

and the corresponding change in the parallel velocity is given by $\Delta v_{\|} = \xi \Delta v$.

In order to calculate the effect of ICRF interaction on the particle trajectories we proceed as follows. Each time the ion passes through the ion cyclotron resonance layer and undergoes resonant interaction with the wave field there is a random change in the perpendicular component of the particle velocity. This incremental change can be readily obtained by integrating the equations of motion over the unperturbed particle trajectories and is given by [1]:

$$\Delta v_{\perp} = \frac{q}{m} \left(\frac{2\pi}{|\dot{\Omega}|} \right)^{1/2} |E_+| e^{-LZ^2} g(Z) \cos\alpha \left[J_{n-1} \left(\frac{k_{\perp} v_{\perp}}{\omega_{ci}} \right) + \frac{E_-}{E_+} J_{n+1} \left(\frac{k_{\perp} v_{\perp}}{\omega_{ci}} \right) \right], \tag{17}$$

where E is the electric field strength with + and - designating the polarized left- and right-handed components, respectively. L is the electric field profile parameter, Z is the distance from the median plane in the vertical direction and α is the phase angle. g(Z) is a function which is used to provide a flat power absorption profile when L = 0. J_n is the Bessel function of order n and $k_{\perp}$ is the perpendicular wave number. The time variation of the cyclotron frequency seen by the drifting ion as it passes through the resonance layer is

$$\dot{\Omega} = \frac{v_{\|} n \omega_{ci} B_{\theta}}{B_{\phi} R} \sin\theta, \tag{18}$$

and

$$\alpha = 2\pi\delta_3, \tag{19}$$

where δ_3 is a uniformly distributed random number between 0 and 1.

The incremental change in the parallel velocity component can be expressed in terms of the change in the perpendicular velocity component as [1]

$$\Delta v_{\|} = k_{\|} v_{\perp} \Delta v_{\perp} / n\omega_{ci}, \tag{20}$$

where $k_{||}$ is the parallel wave number. For an asymmetric wave spectrum the change in $v_{||}$ results in an inward or outward drift for positive and negative sign of $k_{||}$, respectively. For a symmetric spectrum the drift terms cancel and only the diffusion term remains.

The ability of the Monte-Carlo code to reproduce the relevant velocity distribution was tested by comparing it with the semi-analytic model [6] which has previously been tested with the bounce averaged Fokker-Planck code BAFIC [16]. To exclude the orbit effects in HECTOR, flat power absorption, plasma density and temperature profiles were used in the tests. Agreement, within 10%, was found for the minority ion energy content, the mean energy, the participation of the power transferred to background electrons and ions, and the fusion yield. These and other test results can be found in Ref. [10].

Tracing particle orbits using the Monte-Carlo method is computationally expensive. As the minimum orbit following time is determined by the tail formation time, the number of test flights needed becomes important for optimizing CPU time. In peaked profile cases this is particularly difficult due to the introduction of the spatial coordinate in the distribution function which is obtained by integrating the particle trajectories in a finite size ψ grid. To have statistically satisfactory results in a grid expanding over the whole plasma cross-section would require an unreasonable large number of test particles. Thus, in order to have a good resolution in the central region of the discharge we establish the particles initially in the region $0 \leq \psi \leq 0.3$. The sharp gradient in minority ion density at the $\psi = 0.3$ boundary results in an enhanced outward diffusion. However, provided the particle following time is not excessive, an accurate simulation in the very centre of the discharge, $\psi < 0.2$, which is of the greatest interest in terms of ICRF heating efficiency, can be done with a reasonable amount of test particles.

4. RESULTS AND DISCUSSION

4.1 Numerical Considerations and Assumptions

The finite orbit width effects are investigated here using ^{3}He minority scenario in deuterium plasma for JET relevant parameters (Table 1). The electron temperature profile is taken as $T_e = T_{e_o}(1 - 0.9\,\psi)^{P_T}$ and the density profile as $n_e = n_{e_o}(1 - 0.9\,\psi)^{P_n}$, and no impurities are included. To separate the effects on the power absorption profile caused by the finite orbit width and the change in the toroidal angular momentum from that caused by the increase in the Doppler broadening due to increased parallel velocity, we assume the power absorption to take place at $\omega = \omega_c$.

The wave field along the cyclotron resonance is chosen in such a way that at time $t \cong 0$, before the orbit width has expanded, the power deposition profile agrees with the zero orbit width calculations with the PION code [17].

Since the power absorption and transfer profiles are obtained by following test particles in a fixed spatial wave field profile the results can be scaled to other minority densities by keeping the ratio of the total coupled power to the minority density constant. The choice of the minority species is not critical for the modelling of the finite orbit effects, since different species have the same qualitative behaviour.

4.2 Banana Drift and Orbit Effects

To establish the banana drift effect for central ions we first calculated the change in the toroidal angular momentum representing the radial drift (Fig. 3). In this particular case we had the minority ions initially distributed in a region of $0.0 \le \psi \le 0.02$. The energy of these particles starts to increase very quickly due to strong heating, resulting in a widening of the banana orbits and in a rapid decrease in P_ϕ. As the banana drift moves particles to regions with a lower wave field strength and a shorter slowing down time, the rate of increase in the mean energy and consequently the decrease in P_ϕ is reduced. Eventually the mean

energy will reach its peak and starts to decrease. The change in P_ϕ due to RF induced diffusion is initially small but will increase when the mean energy reaches the MeV range. However, the fact that the minority ions are no longer in the regions with high wave field reduces strongly the effect from RF induced diffusion. Pitch angle scattering has little significance for ICRF heated high energy ions, but it is important at the early stages of the tail formation. Here, the banana drift effect was demonstrated using reasonably small peaking factors for the temperature and density profiles while with higher peaking even stronger effects would occur.

In Section 2 we discussed how the inner branch of the banana orbit moves faster towards the high wave field region than the outer branch moves towards the weaker field due to an increase in the perpendicular velocity component, and how the fractional time spent in the resonance layer increases. This would lead to an increased power absorption in the absence of banana diffusion. Figure 4, however, demonstrates that these effects are smaller than that from the banana drift, the net result being a substantial decrease in power absorption, in case C from 40 MW to 20 MW, in a constant wave field compared with zero orbit limit, i.e. $P_{abs}(t = 0)$. The power transfer to the background plasma is also shown to exceed the absorbed power. This occurs because the large fast ion energy content generated at the early stages of heating is later delivered to the outer regions of the plasma where absorption is weak but the slowing down rate fast. Whether the power transfer can become larger than the power absorption depends on the power deposition profile and the amount of coupled power.

Even at moderate heating power levels there is a reduction in the absorbed power due to orbit effects, although this occurs only in a small region in the vicinity of the highest wave field (Fig. 5). However, increasing the power will expand this region and, furthermore, substantial broadening of the power transfer profile will occur. This results in significantly more power transferred

in the outer region of the plasma than is absorbed there, while in the centre of the discharge less power is transferred than is absorbed.

The behaviour of particle orbits during ICRH was discussed in Section 2. Further information to explain the power absorption and transfer profiles can be obtained by examining the minority ion mean energy and density profiles. Because of the finite width of the banana orbits, locally absorbed power produces a radially spread mean energy distribution with a lower high energy tail temperature than that obtained in the zero orbit width limit. Thus, the usual assumption that the mean energy is proportional to the absorbed power density is no longer valid even in the absence of orbit drift and diffusion. The mean energy of the local velocity distribution for different wave field strength is compared with the zero orbit width approximation in Fig. 6. It is to be noted, that the two curves also correspond to different amounts of coupled power since the wave field strength was kept constant.

By studying the evolution of the density profiles in case C (Fig. 7) we found that, at the early stages of heating, the density of minority ions first decreases in the centre of the discharge and consequently increases further out due to orbit broadening. The process continues in time except in the very centre where the density starts to increase again. This increase appears because particles initially further out can reach sufficiently high energy, provided power absorption density is strong enough to form fat banana or D-shape orbits. The inner branch of these orbits can then pass the central region. The density in the centre would indicate substantially higher power absorption density than was obtained. Although some of the ions in the centre region are scattered onto orbits that intersect the resonance layer increasing the power absorption, the majority of these D-shape particle orbits only pass through the centre of the plasma on the low magnetic field side. Thus, they will contribute to the central density, but the interaction with the resonance layer occurs further out in the region of reduced RF power absorption. Similarly, in the outer regions of the

discharge, $\psi > 0.1$, the reduced minority ion density results in less power transferred to background plasma, compared with that obtained with the zero orbit calculations, than the local mean energy would indicate.

A useful quantity which can be calculated, and measured experimentally is the fusion yield from $He^3 + D \rightarrow Li^5 + \gamma$ reaction. The fusion yield has here been expressed in terms of the yield from the reaction $He^3 + D \rightarrow p + He^4$. The latter reaction has a cross-section which is about five orders of magnitude larger but the energy dependence of the two cross-sections is similar. The fusion yield calculated with HECTOR all peaks on the magnetic axis (Fig. 8a). The yield in the zero orbit width limit, also shown in Fig. 8a, peaks off-axis for high power levels due to the particle energy level exceeding the maximum cross-section. Although the spatial distribution of the fusion yield is different for the Monte-Carlo and Fokker-Planck calculations, the total yield for the same amount of coupled power agrees better as can be seen in Fig. 8b.

4.3 Plasma Current Dependency

The deviation of the drift orbit from the magnetic surfaces depends strongly on the plasma current. For low plasma currents ($\cong$ 1 MA) a significant fraction of the energetic ions will intersect the wall. Thus, the plasma will constantly lose the high energy ions are they are heated up. As the plasma current is increased the losses are strongly reduced, and at 5 MA they are negligibly small. ICRF heated high energy particles are strongly trapped and, thus, much less likely to escape the plasma than particles with the same energy in a isotropic distribution. In spite of this, as we saw earlier, the power absorption density in the centre of the discharge is strongly reduced due to orbit effects. In Fig. 9 we compare the total absorbed power for 5 MA and 2 MA plasma currents with the zero orbit calculation which represents the case of the infinite plasma current. The q-profile was kept constant by changing the toroidal magnetic field strength proportional to the plasma current. Even at moderate

input power levels the 5 MA case shows significantly lower absorbed power than that obtained in the zero banana width calculation, and the difference in 2 MA case, is further increased. In the 2 MA case for input power levels exceeding ~ 20 MW the losses of high energy ions is significant and leads to a strong reduction in absorbed power. Projected to future high current plasmas a substantial decrease in absorbed power is indicated. Bearing in mind the flattening of the coupling profiles and the fact that in the experiment situation the absorbed power is kept constant by changing the wave field strength, strong heating outside the centre of the discharge can be anticipated. This is not necessarily a drawback as was demonstrated in the (^{3}He,d) yield calculations, where evenly distributed high power RF heating produced less ions with energy beyond the maximum yield and resulted in higher yield than was obtained by the zero orbit width approximation.

Using a low plasma current, on the other hand, has clear disadvantages. Whereas 5 MA plasma current produced little difference in the fast ion energy, W_{fast} (= $W_\perp$ - $3W_{||}$), compared with $I_p = \infty$ case, the energy content was significantly smaller with the 2 MA current (Fig. 10). Furthermore, although the particle losses out of the plasma were small there was a significant deterioration of the minority ion density in the centre of the discharge (Fig. 11).

4.4 RF Induced Diffusion and Drift

The stochastic change in the resonating ions toroidal angular momentum, due to absorption of toroidal wave momentum, results in a corresponding stochastic change in the minor radius location of the turning points. This random displacement of the turning point was predicted to lead to a spatial diffusion by ICRH [18,19]. The simultaneous diffusion in real and velocity space with more energetic ions diffusing faster in real space, would result in a pump out of high energy ions from regions with high power density. In Section 4.2 we already established the ratio of the effects from banana drift and the RF induced

diffusion and found the latter to be significantly smaller. The comparisons made with the zero orbit width limit represented the combined effects of orbit trapping processes and the banana drift, the latter being difficult to quantify on its own, as it exists even in plasmas with flat temperature and density profiles. The RF induced diffusion and its effects, on the other hand, can be studied by comparing cases with different toroidal mode numbers, the same plasma current, and assuming the position of the absorption to be at $\omega = \omega_c$ in order to exclude the Doppler broadening effect. The density profiles for the toroidal mode numbers $n_\phi = 0$ and $n_\phi = \pm 30$ are shown in Fig. 12. The results confirm the earlier predictions that the finite toroidal mode number leads to further pump out of resonating ions from the centre of the discharge. The RF induced diffusion becomes effective only after the high energy tail has been formed as was seen in Fig. 3. Thus, diffusion due to finite mode number primarily affects the high energy ions. In the 2 MA case, where the confinement of high energy ions already is poor, fewer of these ions are present to undergo diffusion and a smaller effect occurs. The decrease of the maximum mean energy is shown in Fig. 13. This decrease, however, is significantly smaller than that due to orbit effects. The consequent flattening of the power transfer profile and the power absorption profile is shown in Fig. 14.

As future experiments may introduce an asymmetric wave spectrum, we here also demonstrate briefly the associated effects. Again, only the central ions initially distributed in the region of $0.0 \leq \psi \leq 0.02$ in case C are considered. Compared with the banana drift RF induced diffusion was shown in Fig. 3 to be small. In the asymmetric wave spectrum cases the additional inward or outward drift for the positive and negative sign of the toroidal mode number may be large and even exceed the banana drift (Fig. 15). For symmetric spectra the banana drift and the diffusion from pitch angle scattering are outwards. However, in the n_ϕ = -30 case, an inward drift is obtained. If the pitch distribution is displaced towards negative pitch values, friction for passing particles may produce a change in the

toroidal angular momentum large enough to compensate the outward banana drift and a net inward drift occurs. Similarly the pitch angle scattering leads to the formation of an isotropic distribution in pitch giving rise to an increase in P_ϕ. For given particle energy the change in P_ϕ is larger than that produced in the case of a symmetric wave field spectrum. However, it is significantly less than that due to friction and RF interaction. Though the cases of high power density and large toroidal mode number, considered here, may not be typical, nevertheless the introduction of a asymmetric wave spectrum clearly could have significant effects on ICRF heating. A more detailed study of this topic will be presented in a later paper.

5. CONCLUSIONS

A Monte-Carlo code HECTOR has been used to study the effect of finite orbit width on the efficiency of the ICRH in tokamak plasmas. These effects cause a significant reduction in the absorbed power near the magnetic axis where the maximum in the wave power deposition occurs compared with the calculations in which the resonant ion distribution function is obtained from the Fokker-Planck equation in the zero orbit width limit. Furthermore, the power transfer profile becomes substantially broader than the absorption profile.

The finite orbit width also curtails the development of the high energy tail during ICRH. The very high tail energy predicted by Fokker-Planck calculations with zero orbit width is not reached and the mean energy tends to saturate at the centre of the discharge. Although the mean energy profile is significantly flatter than that obtained in the zero orbit width approximation, the total fast ion energy content and the fusion yield for the He^3 minority heating in a D-plasma appear to differ less. However, the chosen parameters were those analysed in Ref. [20], where zero orbit width calculations are compared with JET experimental results showing a good agreement at low power levels. This is somewhat surprising in view of the results obtained here. The finite orbit correction of the

total anisotropic energy content and the total fusion yield is in the direction of decreasing the previous error in the zero orbit width calculations.

Due to the complex nature of the kinetic effects, formulating the orbit correction in the zero orbit approximation is very difficult even in the simplest model cases. One such formulation, a Large-Orbit Model, obtained good agreement with the experimentally measured fast ion energy content [9]. This is again surprising as the correction indicated is substantially larger than the real one calculated with HECTOR using the same plasma parameters. Furthermore, the agreement with the experimental data was reached with HECTOR only after the inclusion of the E_- component of the electric wave field which was neglected in the Large-Orbit Model.

The spatial diffusion due to absorption of waves with a finite toroidal wave number could be confirmed by comparing the density profiles of cases with zero and finite toroidal mode number. However, this effect is strongly reduced by the banana drift which effectively moves high energy ions away from the centre of the discharge. For small plasma current the deviation of the density profile between cases with and without zero toroidal mode number was smaller due to an already poor confinement of high energy ions in the centre region in the absence of toroidal propagation of the waves. An example of an asymmetric wave spectrum indicates the existence of a strong RF induced drift.

The existence of the finite orbit width effects is not limited to large tokamaks with high RF power, these effects also exist in situations where moderate power is coupled to a small minority ion concentration. Finite orbit effects will be in evidence in future large machines where their correct optimisation is vital for the effective heating regimes by ICRF.

Acknowledgements

The authors appreciate the constructive comments of Dr. T.E. Stringer. M.A. Kovanen also wants to thank JET Theory Division for hospitality, and the

Finnish Cultural Foundation and the Trust of Emil Aaltonen for financial support.

References

[1] Stix, T.H., Nucl. Fusion 15 (1975) 737.

[2] Harvey, R.W., McCoy, M.G., Kerbel, G.D., Chiu, S.C., Nucl. Fusion 26 (1986) 43.

[3] Chiu, S.C., Phys. Fluids 28 (1985) 1371.

[4] Chang, C.S., Phys. Fluids 28 (1985) 3598.

[5] Chang, C.S., Colestock, P., Phys. Fluids 2 (1990) 310.

[6] Anderson, D., Core, W., Eriksson, L.-G., Hamnén, H., Hellsten, T., Lisak, M., Nucl. Fusion 27 (1987) 911.

[7] Kesner, J., Nucl. Fusion 18 (1978) 781.

[8] Kerbel, G.D., McCoy, M.G., Phys. Fluids 28 (1985) 3629.

[9] Cottrell, G.A., Start, D.F., A large-orbit model for ICRH heating: Comparison with JET data, JET-P(90)17, JET Joint Undertaking, (1990), submitted to Nuclear Fusion.

[10] Kovanen, M.A., Core, W.G.F., HECTOR - A code for the study of charged particles in axisymmetric tokamak plasmas, JET-R(88)01 and JET-P(90)40, JET Joint Undertaking (1990), submitted to J. Comput. Phys.

[11] Core, W.G.F., Nucl. Fusion 7 (1989) 1101.

[12] Hellsten, T., Plasma Phys. and Controlled Fusion 31 (1989) 1391.

[13] Stix, T.H., private communication.

[14] Boozer, A.H., Kuo-Petravic, G., Phys. Fluids 24 (1981) 851.

[15] Spitzer, L. Jr., The Physics of Fully Ionized Gases, 2nd Revised Ed., Interscience, New York (1962).

[16] Succi, S., Appert, K., Core, W., Hamnén, H., Hellsten, T., Vaclavik, J., Comp. Phys. Comm. 40 (1986) 137.

[17] Eriksson, L.-G., Hellsten, T., Self-consistent calculations of ICRH power deposition and velocity distribution, JET-P(89)65, JET Joint Undertaking (1989), submitted to Nucl. Fusion.

[18] Riyopoulos, S, Tajima, T., Hatori, T., Pfirsch, D., Nucl. Fusion 26 (1986) 627.

[19] Chen, L, Vaclavik, J, Hammett, G.W., Nucl. Fusion 28 (1988) 389.

[20] Eriksson, L.-G., Hellsten, T., Boyd, D.A., Nucl. Fusion 29 (1989) 87.

TABLE 1

Plasma Parameters for the Reference Discharge

Major radius, R_o	2.96 m
Minor radius, a	1.20 m
Electron density on axis, n_{e_o}	5×10^{19}m-3
Electron density profile parameter, p_n	0.5
Electron temperature on axis, T_{e_o}	8 keV
Electron temperature profile parameter, p_T	1.0
Magnetic field at $R = R_o$, B_ϕ	3.4T
Plasma current, I_p	2 MA, 5 MA
^{3}He minority concentration, $n_{^3He}/n_e$	3%
Electric field profile parameter, L	16.0
Perpendicular mode number $n_\perp$	0
Toroidal mode number n_ϕ	0, 30
Frequency, f	33 MHz
The input power, P_{IN}:	
Case A	2.5 MW
Case B	10.0 MW
Case C	40.0 MW

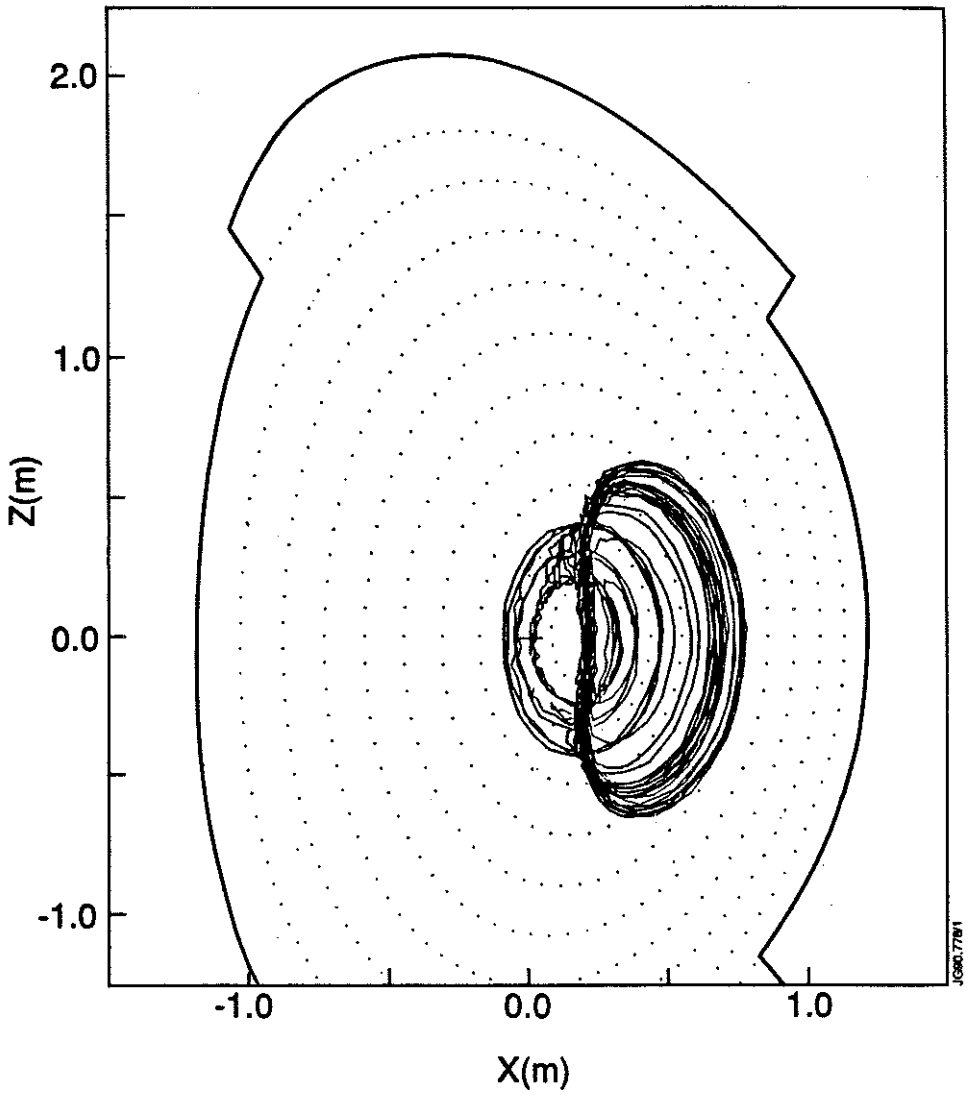

Fig. 1 A trajectory of a single ^{3}He ion during ICRH.

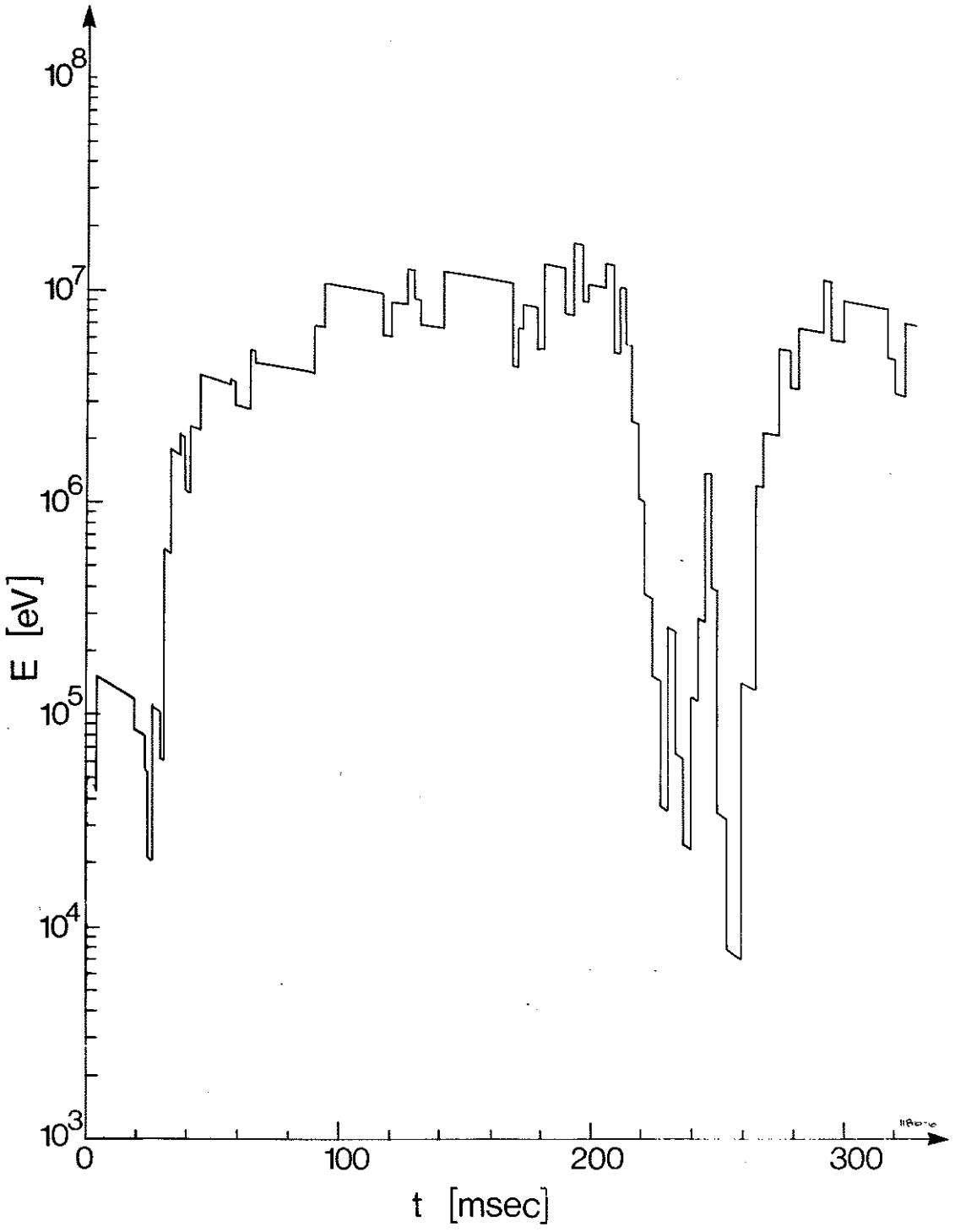

Fig. 2 The change in energy of the ^{3}He test particle due to Coulomb collisions and RF-interactions. The steady decrease in energy between the RF-interactions is due to slowing down on electrons.

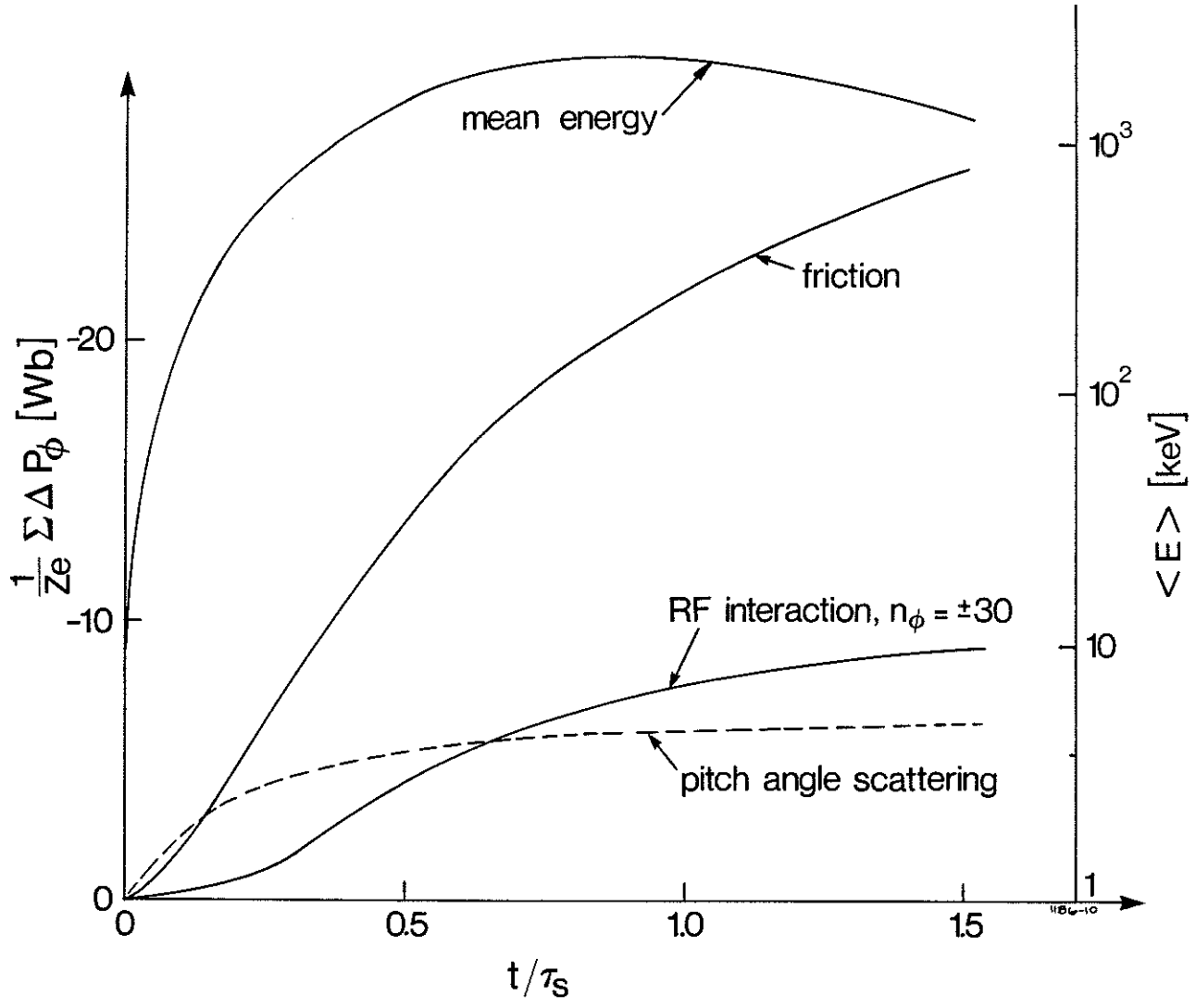

Fig. 3 The total change in the toroidal angular momentum as a function of time due to banana orbit drift, pitch angle scattering and RF induced diffusion in the case of a symmetric wave field spectrum. A contribution from each test particle have been added together. The mean energy is also shown.

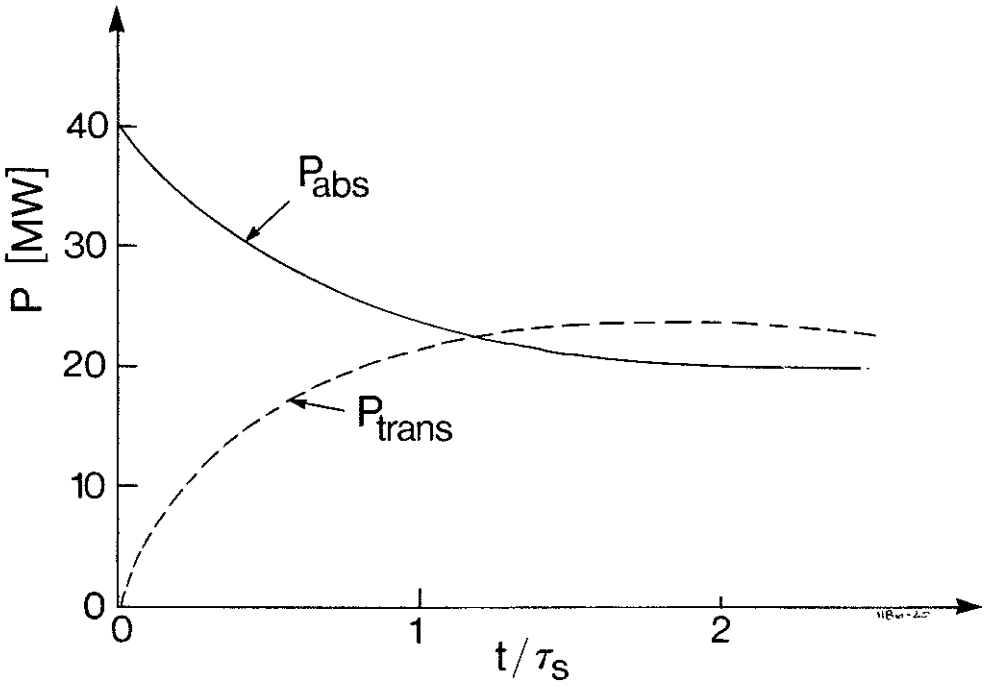

Fig. 4 Time evolution of the total absorbed power and power transferred to the background plasma species in case C.

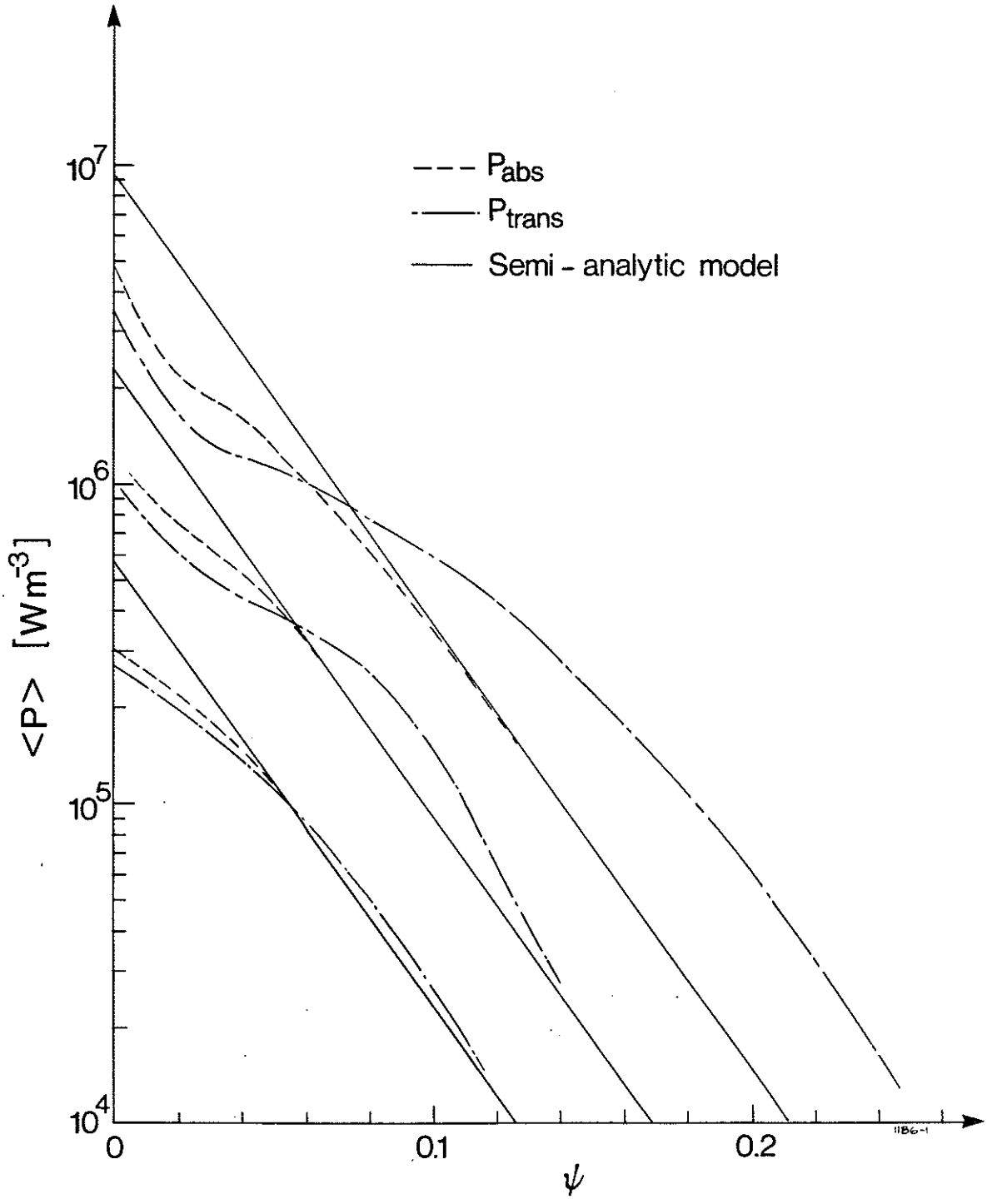

Fig. 5 Power absorption and transfer profiles for 5 MA plasma current in cases A, B and C, compared with the power absorption profile in the zero banana width approximation.

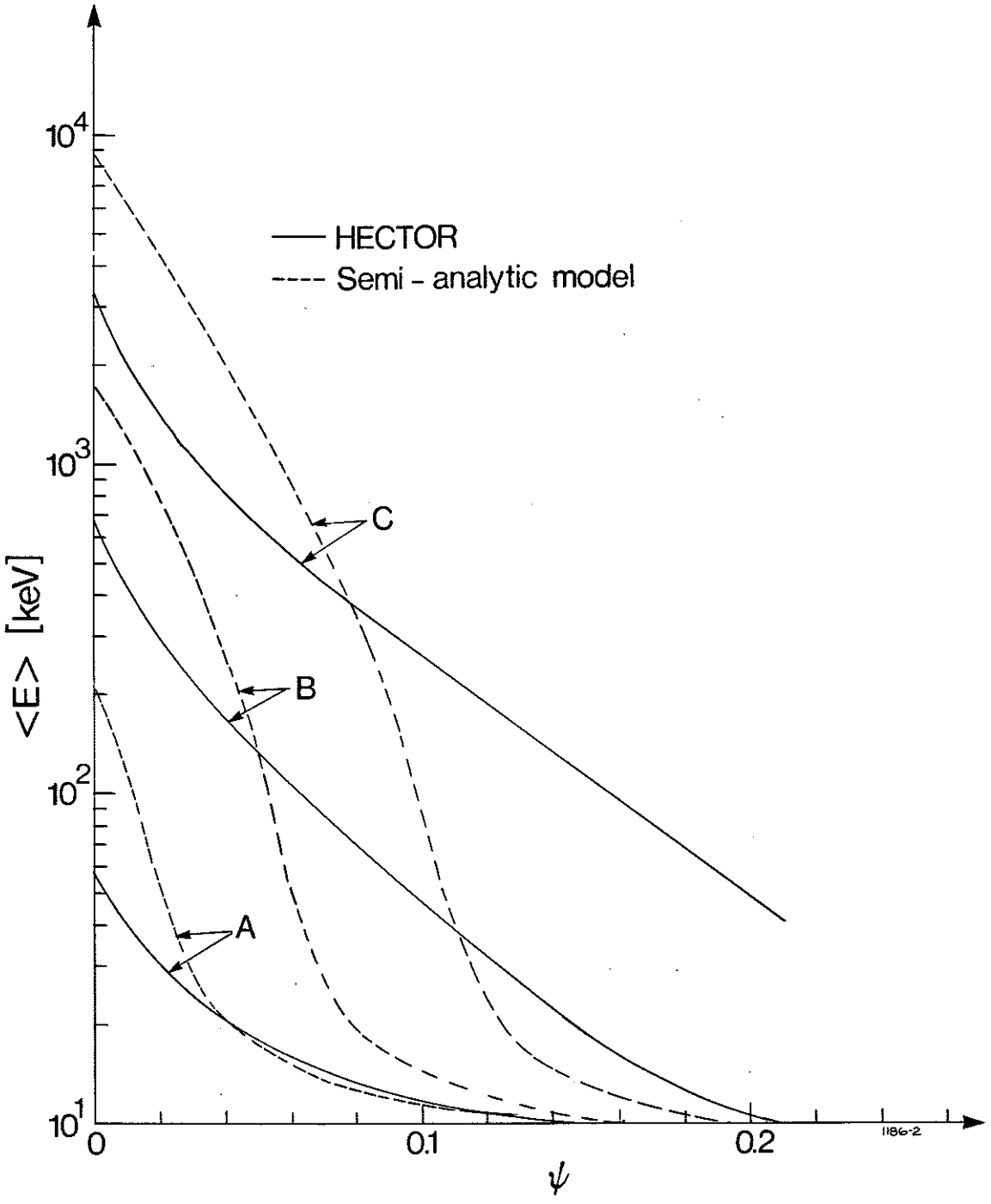

Fig. 6 Mean energy of resonating ions versus ψ for the three cases with 5 MA plasma current compared with Fokker-Planck calculations with the same strength of the wave field.

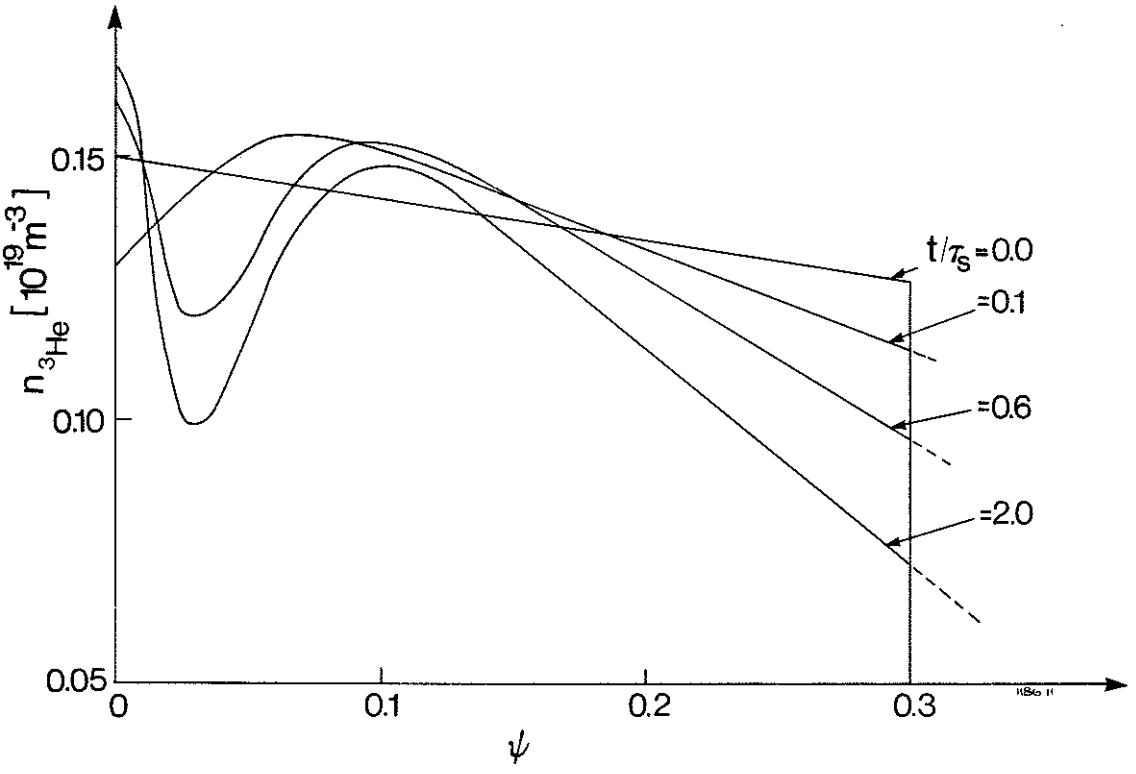

Fig. 7 Minority ion density profiles near the centre in the case C for 5 MA plasma current at t = 0, 0.1, 0.6 and 2 t_s.

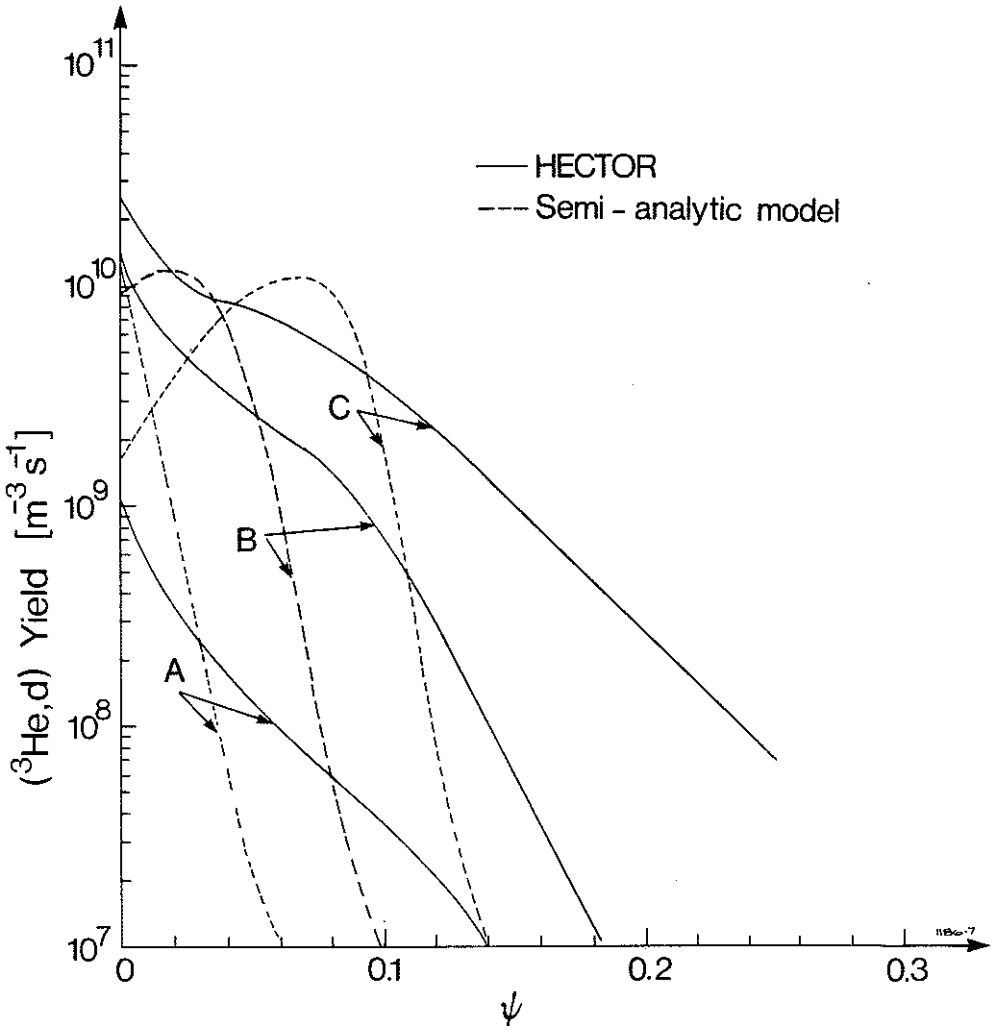

Fig. 8a Fusion yield due to the $He^3 + D \rightarrow He^4 + H$ reaction versus ψ for the three cases. Comparison of HECTOR with 5 MA plasma current with Fokker-Planck calculations is made for the same field strength.

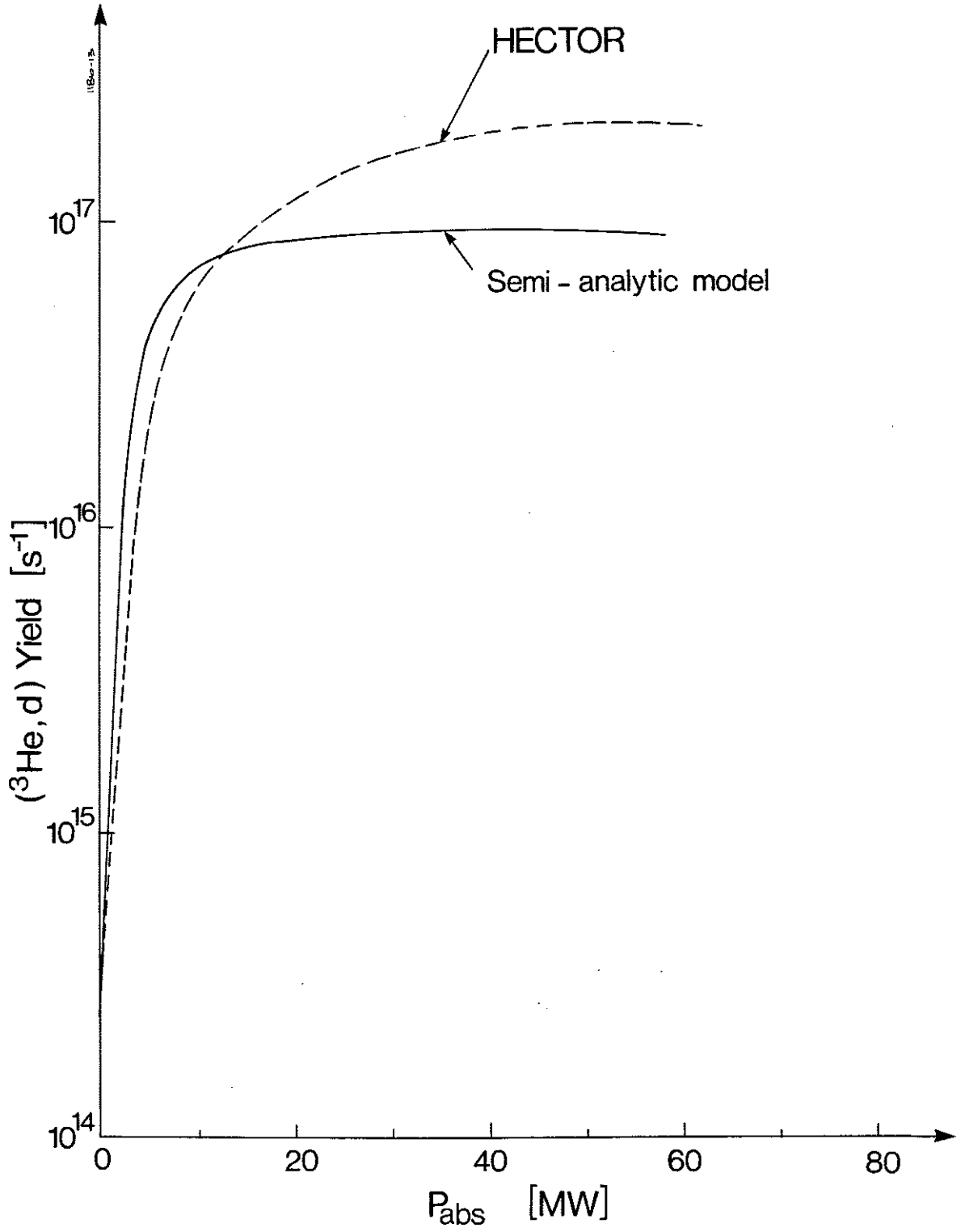

Fig. 8b Total fusion yield versus coupled power from HECTOR with 5 MA plasma current, compared with zero orbit width Fokker-Planck calculations.

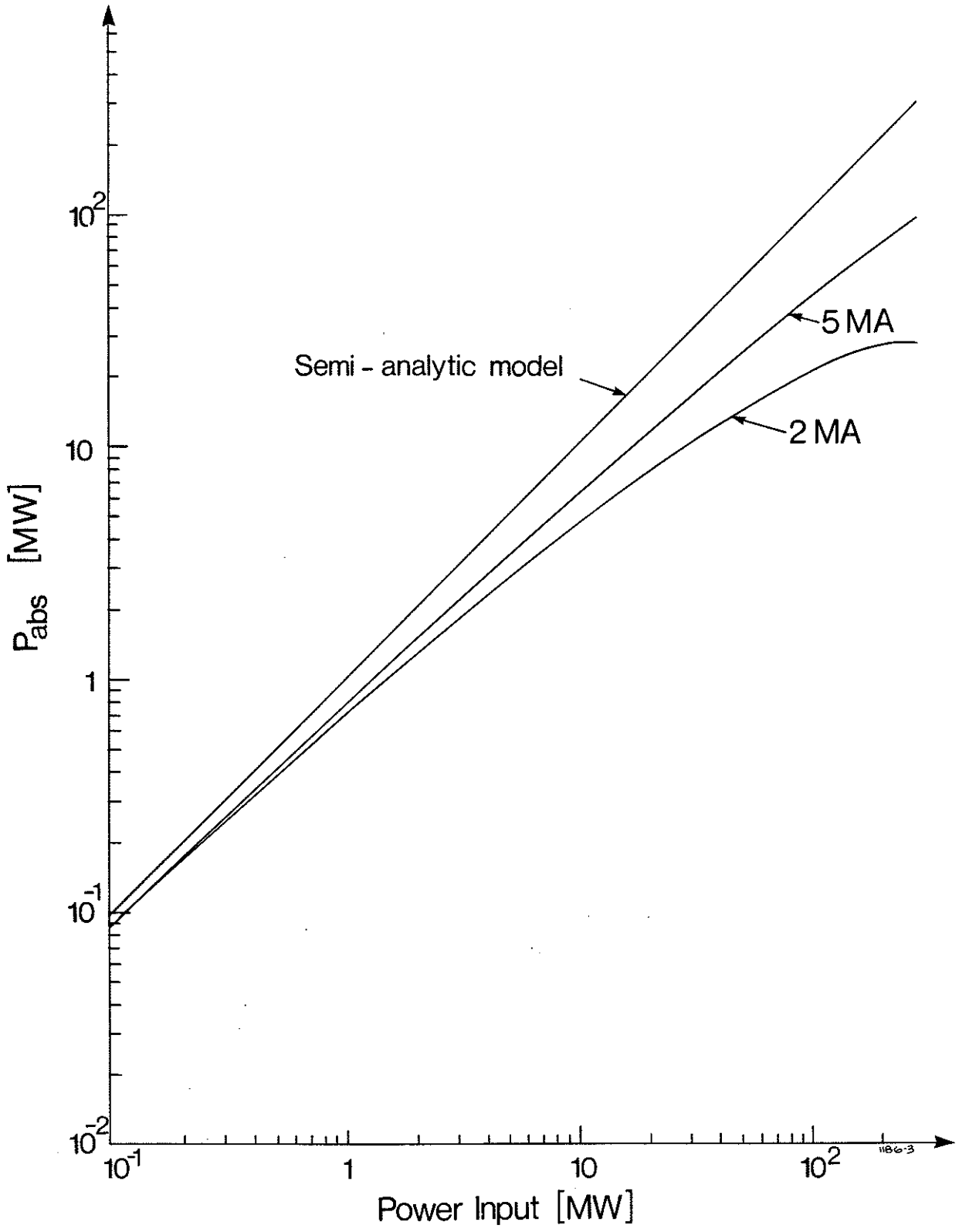

Fig. 9 Total absorbed power versus the input power for 2 MA and 5 MA plasma currents compared with the zero orbit width Fokker-Planck calculations. The results from HECTOR are after slowing down time.

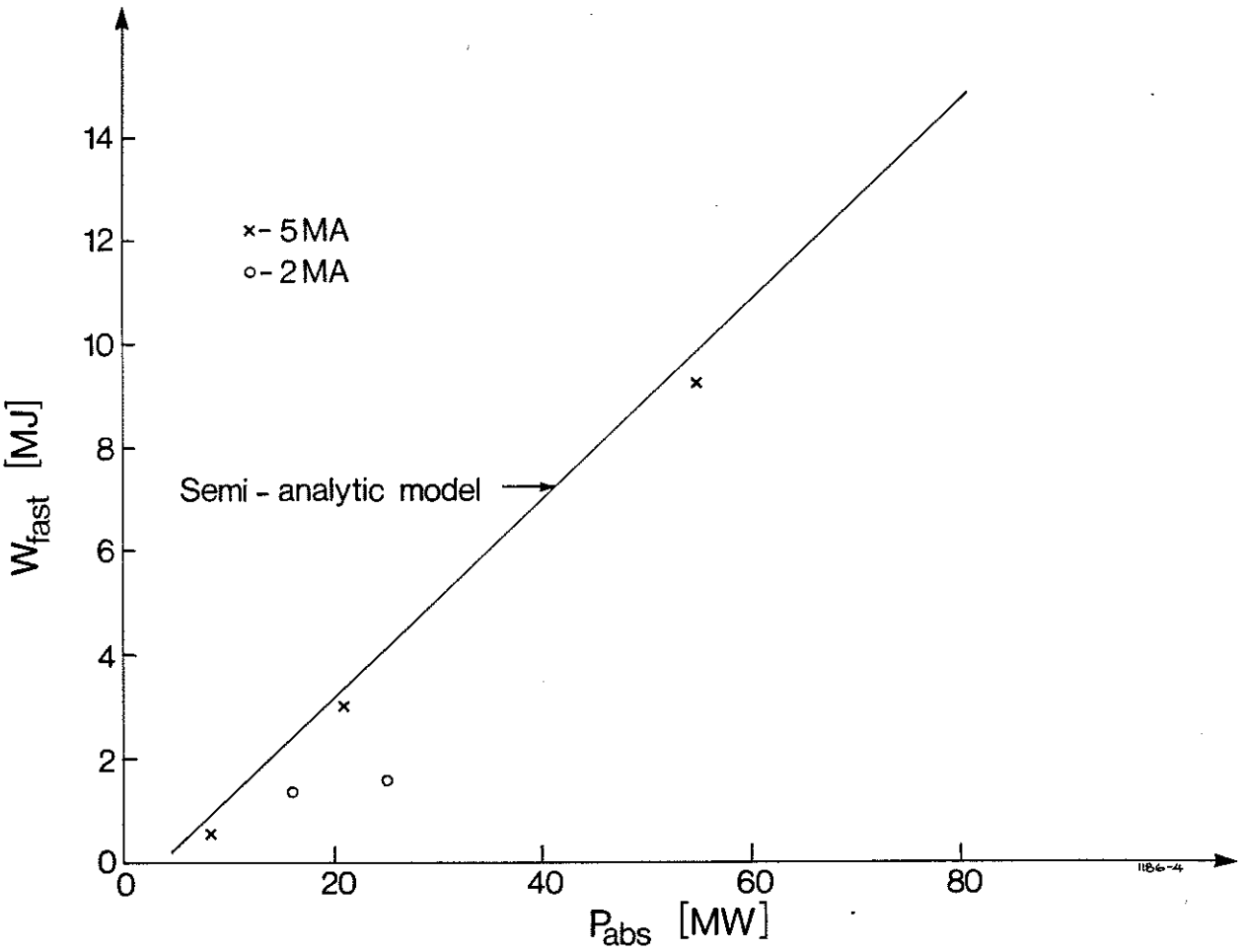

Fig. 10 Total energy content of resonating ions versus total coupled power. X and O are HECTOR calculations, full-line from zero orbit width Fokker-Planck calculations.

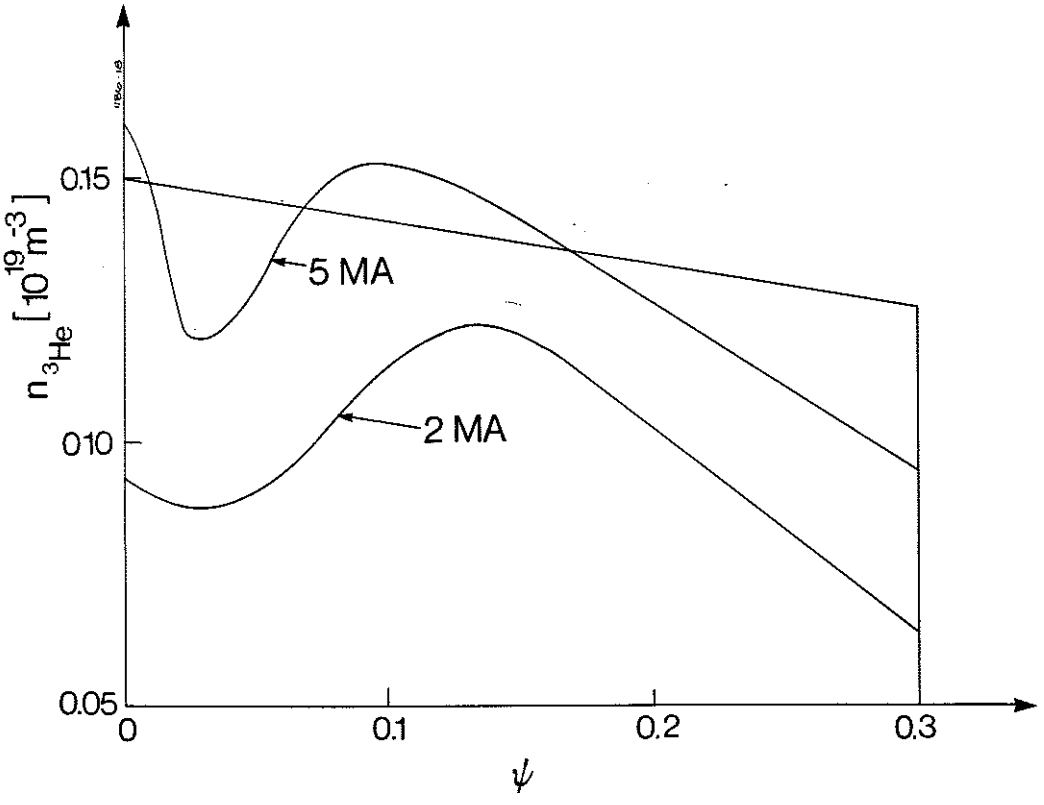

Fig. 11 Comparison of minority ion density profiles for 2 MA and 5 MA plasma currents.

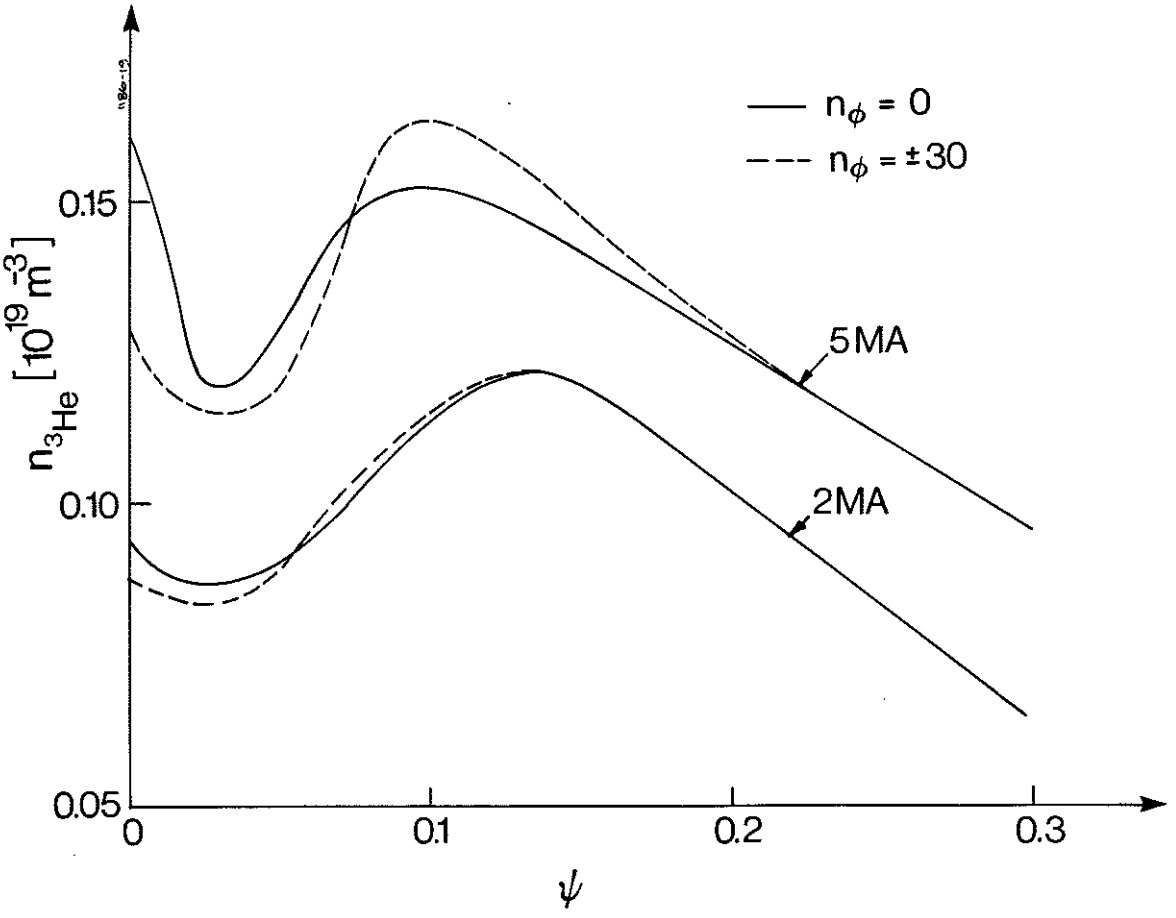

Fig. 12 Comparison of minority ion density profiles for 5 MA and 2 MA plasma currents with toroidal mode numbers $n_\phi = 0$ and $n_\phi = \pm 30$.

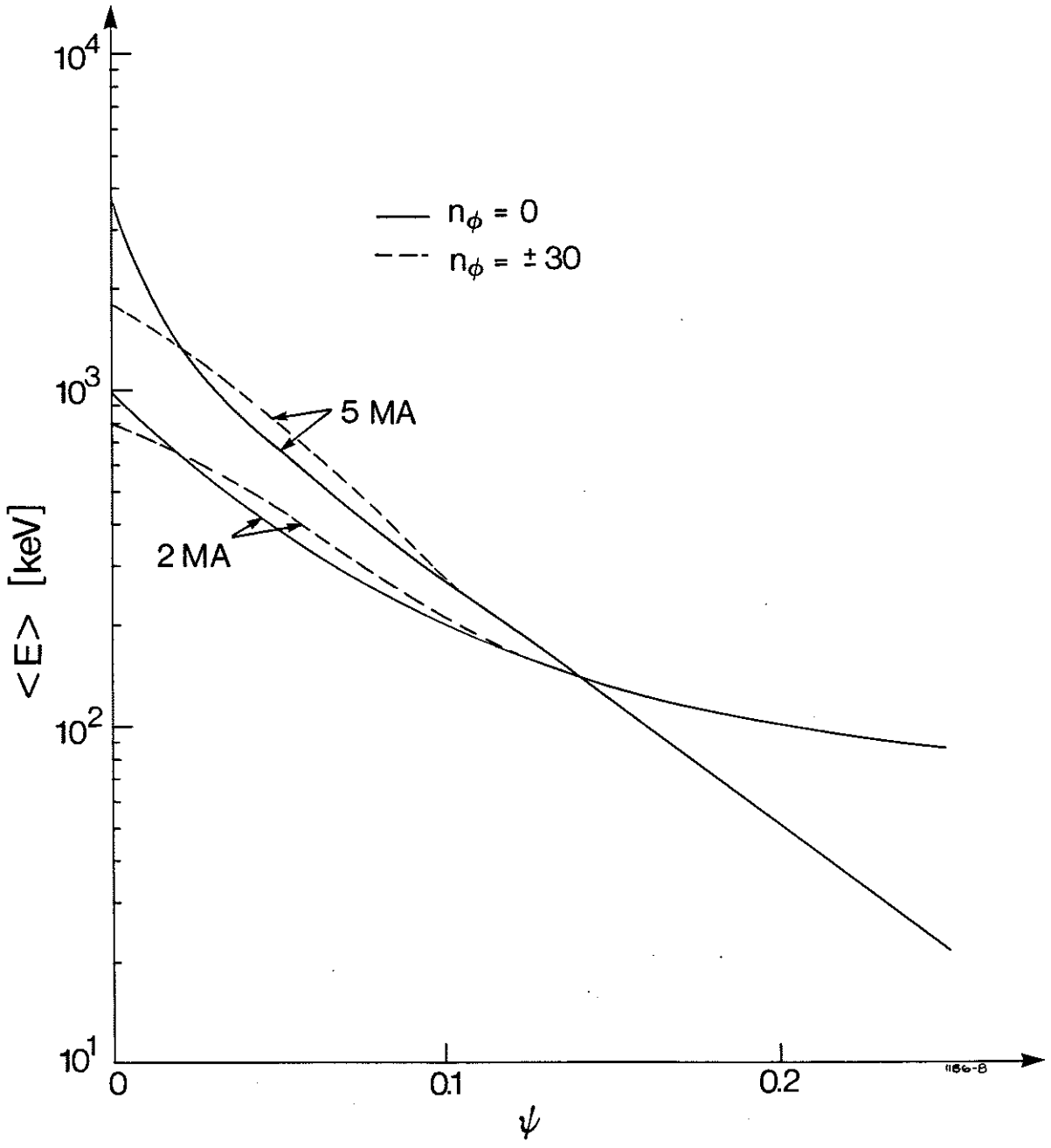

Fig. 13 Comparison of the mean energy profiles for 2 MA and 5 MA plasma currents with toroidal mode numbers $n_\phi = 0$ and $n_\phi = \pm 30$.

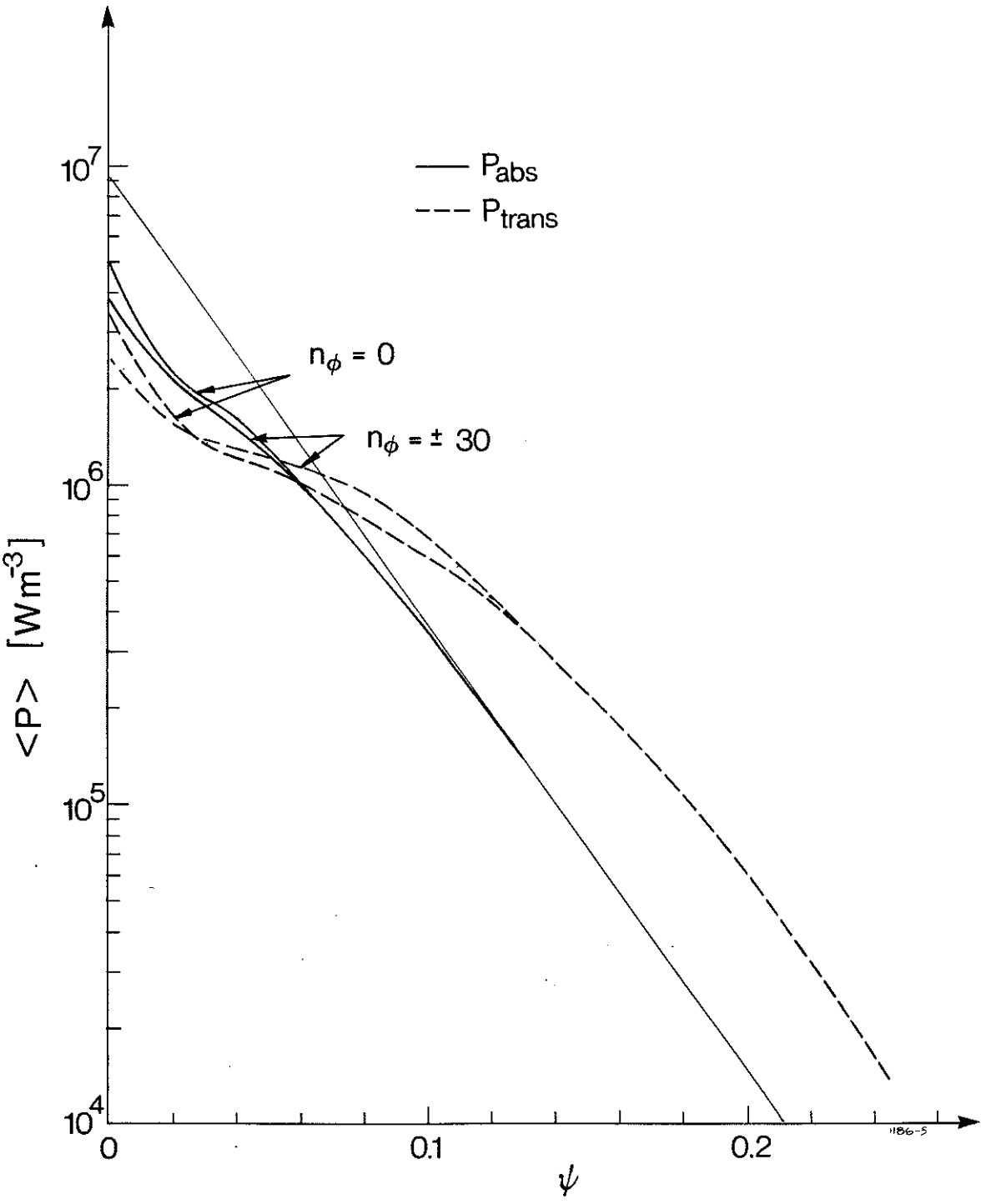

Fig. 14 Power absorption and transfer profiles in case C with 5 MA plasma current for toroidal mode numbers $n_\phi = 0$ and $n_\phi = \pm 30$.

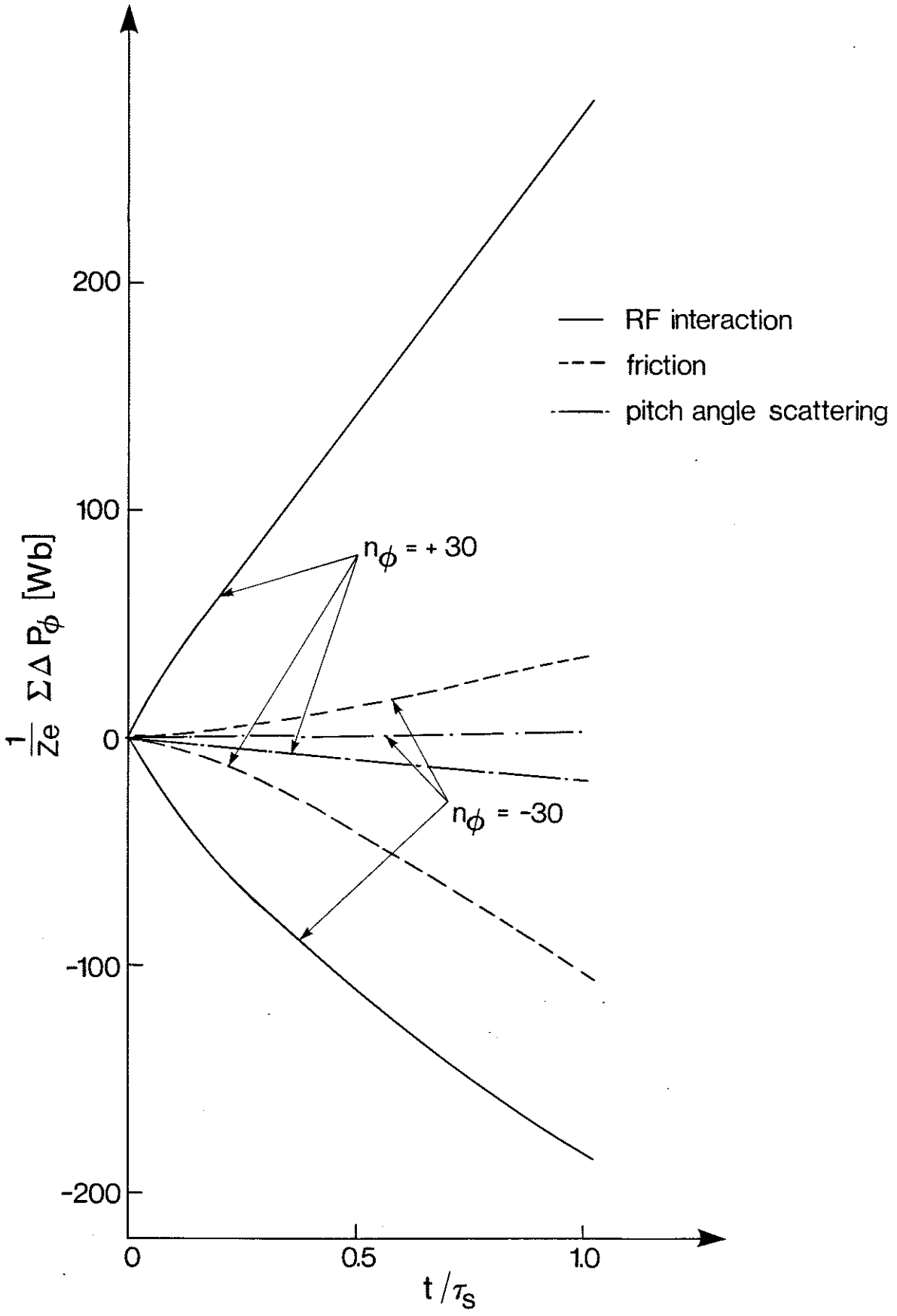

Fig. 15 The total change in the toroidal angular momentum as a function of time due to banana orbit drift, pitch angle scattering and RF induced diffusion and drift in the case of an asymmetric wave field spectrum. A contribution from each test particle have been added together.

APPENDIX 1.

THE JET TEAM

JET Joint Undertaking, Abingdon, Oxon, OX14 3EA, U.K.

J.M.Adams[1], F.Alladio[4], H.Altmann, R.J.Anderson, G.Appruzzese, W.Bailey, B.Balet, D.V.Bartlett, L.R.Baylor[24], K.Behringer, A.C.Bell, P.Bertoldi, E.Bertolini, V.Bhatnagar, R.J.Bickerton, A.Boileau[3], T.Bonicelli, S.J.Booth, G.Bosia, M.Botman, D.Boyd[31], H.Brelen, H.Brinkschulte, M.Brusati, T.Budd, M.Bures, T.Businaro[4], H.Buttgereit, D.Cacaut, C.Caldwell-Nichols, D.J.Campbell, P.Card, J.Carwardine, G.Celentano, P.Chabert[27], C.D.Challis, A.Cheetham, J.Christiansen, C.Christodoulopoulos, P.Chuilon, R.Claesen, S.Clement[30], J.P.Coad, P.Colestock[6], S.Conroy[13], M.Cooke, S.Cooper, J.G.Cordey, W.Core, S.Corti, A.E.Costley, G.Cottrell, M.Cox[7], P.Cripwell[13], F.Crisanti[4], D.Cross, H.de Blank[16], J.de Haas[16], L.de Kock, E.Deksnis, G.B.Denne, G.Deschamps, G.Devillars, K.J.Dietz, J.Dobbing, S.E.Dorling, P.G.Doyle, D.F.Düchs, H.Duquenoy, A.Edwards, J.Ehrenberg[14], T.Elevant[12], W.Engelhardt, S.K.Erents[7], L.G.Eriksonn[5], M.Evrard[2], H.Falter, D.Flory, M.Forrest[7], C.Froger, K.Fullard, M.Gadeberg[11], A.Galetsas, R.Galvao[8], A.Gibson, R.D.Gill, A.Gondhalekar, C.Gordon, G.Gorini, C.Gormezano, N.A.Gottardi, C.Gowers, B.J.Green, F.S.Griph, M.Gryzinski[26], R.Haange, G.Hammett[6], W.Han[9], C.J.Hancock, P.J.Harbour, N.C.Hawkes[7], P.Haynes[7], T.Hellsten, J.L.Hemmerich, R.Hemsworth, R.F.Herzog, K.Hirsch[14], J.Hoekzema, W.A.Houlberg[24], J.How, M.Huart, A.Hubbard, T.P.Hughes[32], M.Hugon, M.Huguet, J.Jacquinot, O.N.Jarvis, T.C.Jernigan[24], E.Joffrin, E.M.Jones, L.P.D.F.Jones, T.T.C.Jones, J.Källne, A.Kaye, B.E.Keen, M.Keilhacker, G.J.Kelly, A.Khare[15], S.Knowlton, A.Konstantellos, M.Kovanen[21], P.Kupschus, P.Lallia, J.R.Last, L.Lauro-Taroni, M.Laux[33], K.Lawson[7], E.Lazzaro, M.Lennholm, X.Litaudon, P.Lomas, M.Lorentz-Gottardi[2], C.Lowry, G.Magyar, D.Maisonnier, M.Malacarne, V.Marchese, P.Massmann, L.McCarthy[28], G.McCracken[7], P.Mendonca, P.Meriguet, P.Micozzi[4], S.F.Mills, P.Millward, S.L.Milora[24], A.Moissonnier, P.L.Mondino, D.Moreau[17], P.Morgan, H.Morsi[14], G.Murphy, M.F.Nave, M.Newman, L.Nickesson, P.Nielsen, P.Noll, W.Obert, D.O'Brien, J.O'Rourke, M.G.Pacco-Düchs, M.Pain, S.Papastergiou, D.Pasini[20], M.Paume[27], N.Peacock[7], D.Pearson[13], F.Pegoraro, M.Pick, S.Pitcher[7], J.Plancoulaine, J-P.Poffé, F.Porcelli, R.Prentice, T.Raimondi, J.Ramette[17], J.M.Rax[27], C.Raymond, P-H.Rebut, J.Removille, F.Rimini, D.Robinson[7], A.Rolfe, R.T.Ross, L.Rossi, G.Rupprecht[14], R.Rushton, P.Rutter, H.C.Sack, G.Sadler, N.Salmon[13], H.Salzmann[14], A.Santagiustina, D.Schissel[25], P.H.Schild, M.Schmid, G.Schmidt[6], R.L.Shaw, A.Sibley, R.Simonini, J.Sips[16], P.Smeulders, J.Snipes, S.Sommers, L.Sonnerup, K.Sonnenberg, M.Stamp, P.Stangeby[19], D.Start, C.A.Steed, D.Stork, P.E.Stott, T.E.Stringer, D.Stubberfield, T.Sugie[18], D.Summers, H.Summers[20], J.Taboda-Duarte[22], J.Tagle[30], H.Tamnen, A.Tanga, A.Taroni, C.Tebaldi[23], A.Tesini, P.R.Thomas, E.Thompson, K.Thomsen[11], P.Trevalion, M.Tschudin, B.Tubbing, K.Uchino[29], E.Usselmann, H.van der Beken, M.von Hellermann, T.Wade, C.Walker, B.A.Wallander, M.Walravens, K.Walter, D.Ward, M.L.Watkins, J.Wesson, D.H.Wheeler, J.Wilks, U.Willen[12], D.Wilson, T.Winkel, C.Woodward, M.Wykes, I.D.Young, L.Zannelli, M.Zarnstorff[6], D.Zasche[14], J.W.Zwart.

PERMANENT ADDRESS

1. UKAEA, Harwell, Oxon. UK.
2. EUR-EB Association, LPP-ERM/KMS, B-1040 Brussels, Belgium.
3. Institute National des Récherches Scientifique, Quebec, Canada.
4. ENEA-CENTRO Di Frascati, I-00044 Frascati, Roma, Italy.
5. Chalmers University of Technology, Göteborg, Sweden.
6. Princeton Plasma Physics Laboratory, New Jersey, USA.
7. UKAEA Culham Laboratory, Abingdon, Oxon. UK.
8. Plasma Physics Laboratory, Space Research Institute, Sao José dos Campos, Brazil.
9. Institute of Mathematics, University of Oxford, UK.
10. CRPP/EPFL, 21 Avenue des Bains, CH-1007 Lausanne, Switzerland.
11. Risø National Laboratory, DK-4000 Roskilde, Denmark.
12. Swedish Energy Research Commission, S-10072 Stockholm, Sweden.
13. Imperial College of Science and Technology, University of London, UK.
14. Max Planck Institut für Plasmaphysik, D-8046 Garching bei München, FRG.
15. Institute for Plasma Research, Gandhinagar Bhat Gujat, India.
16. FOM Instituut voor Plasmafysica, 3430 Be Nieuwegein, The Netherlands.
17. Commissiariat à L'Energie Atomique, F-92260 Fontenay-aux-Roses, France.
18. JAERI, Tokai Research Establishment, Tokai-Mura, Naka-Gun, Japan.
19. Institute for Aerospace Studies, University of Toronto, Downsview, Ontario, Canada.
20. University of Strathclyde, Glasgow, G4 ONG, U.K.
21. Nuclear Engineering Laboratory, Lapeenranta University, Finland.
22. JNICT, Lisboa, Portugal.
23. Department of Mathematics, Univeristy of Bologna, Italy.
24. Oak Ridge National Laboratory, Oak Ridge, Tenn., USA.
25. G.A. Technologies, San Diego, California, USA.
26. Institute for Nuclear Studies, Swierk, Poland.
27. Commissiariat à l'Energie Atomique, Cadarache, France.
28. School of Physical Sciences, Flinders University of South Australia, South Australia SO42.
29. Kyushi University, Kasagu Fukuoka, Japan.
30. Centro de Investigaciones Energeticas Medioambientales y Techalogicas, Spain.
31. University of Maryland, College Park, Maryland, USA.
32. University of Essex, Colchester, UK.
33. Akademie de Wissenschaften, Berlin, DDR.

CR 88.49.1A